Bioinsp. Biomim. **3** (2008) 035007 (10pp) doi:10.1088/1748-3182/3/3/035007

Biomaterial-based infrared detection

O Yavuz and M Aldissi

Fractal Systems, Inc., 200 9th Avenue North, Suite 100, Safety Harbor, FL 34695, USA

E-mail: maldissi@fractalsystemsinc.com

Received 13 February 2008
Accepted for publication 13 May 2008
Published 31 July 2008
Online at stacks.iop.org/BB/3/035007

Abstract

This effort is focused on the use of crustacyanin protein extracted from the lobster shell in IR detection and imaging applications. In addition to the protein's excellent reversible thermo-active response in the IR region of interest, electrical characteristics versus temperature showed that the protein can be used as an electro-optic thermal sensing device as well. The high sensitivity and fast response of the protein layer were further enhanced by the deposition process we used. The thin coatings were prepared by Langmuir–Blodgett and self-assembly techniques. Furthermore, the protein exhibited temperature variation under Ti:sapphire laser excitation at different wavelengths in ambient environment. We have also shown that the protein exhibits fluorescence properties after exposure to IR heat. Stability of the protein, which is important in this type of application, was also demonstrated using the different characterization techniques after repeated heating/cooling cycles. We can conclude that this protein represents a formidable candidate for the fabrication of IR sensors and microbolometers for uncooled IR imaging applications.

(Some figures in this article are in colour only in the electronic version)

1. Introduction

Infrared (IR) imaging systems constitute a key factor of military superiority. In the modern battlefield, IR systems are engaged in a wide variety of applications, such as ground or air and space based surveillance and targeting systems, weapon night sights, aircraft navigation and piloting night fire control systems. The heart of each IR imaging system is the detector array, which is usually based on a semiconductor sensitive to the low-energy IR photons. Progress in the imaging systems is very closely related to the progress of the IR/thermal detector technology. There are four detector technologies that may meet some of the specifications of third-generation IR systems: HgCdTe, antimonide-based compounds, quantum well IR photodetectors and uncooled microbolometer detectors. Three of the most common thermal detectors include the bolometers [1, 2], thermopiles [3, 4] and pyroelectric [5] detectors. Bolometers are generally easier to fabricate than pyroelectric detectors and have better responses than thermopiles. However, their operation is significantly affected by generation of self-heating when current is passed through the device for readout [6].

Current uncooled detectors and imaging systems are extremely expensive, rigid, hard to produce at high yield and require exotic materials and processes for their fabrication. Therefore, there is great interest in the development of other materials in general and of bio-inspired materials in particular, which is the subject of our effort, for the development of lightweight, low-cost uncooled thermal/IR detectors.

As proteins are highly self-absorbing materials in the 3–5 and 8–12 μm regions, no additional IR absorbing coating is required to achieve efficient radiation resulting with the reduction of both thermal capacitance and conductance. In addition to low thermal capacitance and conductance, the readout mechanisms of proteins are relatively faster than the inorganic or polymeric materials. These advantages make protein-based microbolometer technology very promising for a number of civilian and military applications ranging from night vision, thermal imaging, biological diagnostics and fire detection.

Since thermal sensors rely on temperature changes of the temperature-sensitive element due to IR absorption rather than on photo-excitation of carriers, they can operate at room temperature with little wavelength dependence of the response over a wide IR spectral range at low cost. To meet such requirements with biologically inspired molecules, we have investigated with a material perspective how biological materials can sense thermal/IR radiation for use in uncooled

imaging systems. The present work focuses on the study of a carotenoid-crustacyanin, which exists in nature in uncooled IR detectors through dehydration and rehydration processes. Therefore, α-crustacyanin (α-CRY) and β-crustacyanin (β-CRY) pigments were extracted and purified from *Homarus Americanus*. The synthetic recombinant technique was also applied to clone and express CRY for comparison purposes.

After successful extraction and synthesis of materials, thin films of the soluble materials are fabricated using the self-assembly (SA) and Langmuir–Blodgett (LB) techniques, which are very simple and of low cost compared to techniques currently used for conventional materials such as chemical vapor deposition, pulsed laser deposition or laser induced chemical vapor deposition. Such controlled processing techniques allow growing thin molecular films. LB films are mechanically assembled arrays of amphiphillic molecules upon a water surface. Once the molecules are compressed to the desired organization, the film can then be transferred to a variety of pre-treated substrates including silicon.

2. Experimental details

2.1. Synthesis and extraction of materials

Histidine (HST) (*N*-α-acetoxy-DL-histidine hydrate) is studied as a reference for comparison with the spectra of astaxanthin (AXT) in α-CRY. AXT and HST were purchased from Aldrich. The synthetic recombinant technique is applied to clone and express CRY as follows.

2.1.1. Cloning of the target gene (β-CRY) into an expression vector pET21a. The target gene β-CRY was released by BamHI+XhoI from pCR2.1 and gel purified using the gel purification kit (Qiagen). The vector pET21a was cut with the same enzymes and was gel purified as well. The ligation reaction was carried as follows:

Insert (β-CRY)	5μl	Vector (pET21a)	3 μl
10$\times$ ligation buffer	1μl	T4 DNA ligase (NEB)	1μl

The ligation mixture was incubated at 4 °C overnight. Transformation was done using DH5α competent cells. Briefly, competent cells were thawed from −80 °C in ice; the ligation mixture was gently mixed with the competent cells. After incubation on ice for 30 min, the competent cells were subject to a heat shock at 37 °C for 5 min and put back on ice for 3 min. 750 μl of LB medium without ampicillin was added to the competent cells and incubated at 37 °C for 30 min with gentle shaking. The competent cells were then spread onto a 10 cm agar plate with ampicillin (100 μg ml^{-1}) and incubated at 37 °C overnight. Small colonies were visible the next morning, and single colonies were picked and incubated in 2 ml of ampicillin-containing LB medium at 37 °C with shaking (300 rpm) overnight. Mini-preparations of plasmid were made using the mini preparation kit from Qiagen. The preparations were identified by BamHI+XhoI digestion. One of the positive plasmid clones was transformed into BL21 cells for expression.

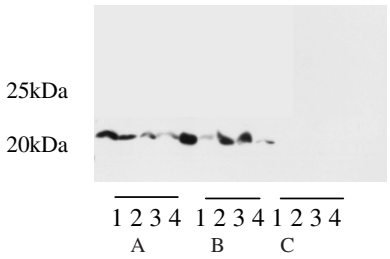

Figure 1. Mini-induction. Western blot using anti-His antibody: A, before induction; B, pellet after induction and C, lysate after induction; Clone 1 was chosen for large-scale expression and purification.

2.1.2. Expression and purification. *Test expression*: four colonies from the transformed BL21 cells were grown in 5 ml of LB with ampicillin at room temperature overnight. IPTG was added to a final concentration of ∼0.5 mM to induce protein expression. After 3 h, *E. coli* cells were harvested by centrifugation at 5000 rpm for 10 min. Cells were lyzed by a lysis buffer (50 mM NaH_2PO_4, 300 mM NaCl, 10 mM imidazole, 1% Trotin-X100, pH = 8.0, protease inhibitors cocktail). After centrifugation at 10 000*g* for 10 min, the supernatant and pellet fractions were subjected to western blot using anti-HIS antibody (figure 1). It seems that most of the protein is in the pellet fraction.

Large-scale expression and purification: clone 1 from the test expression was chosen for large-scale expression. Overnight culture of clone 1 was carried out in 10 ml of LB with ampicillin. The next morning, the 10 ml culture was added to 1 L of fresh LB medium with ampicillin, and continued to grow for 4 h till the OD600 reached 0.8. IPTG was added to a final concentration of ∼0.5 mM, and continue to grow for 3 h. Cells were harvested by centrifuge at 5000 rpm for 10 min, washed twice with PBS (pH = 7.5) and lyzed with lysis buffer, and the soluble and non-soluble fractions were separated by centrifugation. Both the soluble and the non-soluble fractions were purified. Purification was carried out according to standard procedures (Ni-NTA resin, Qiagen). The protein was eluted with an elution buffer (50 mM NaH_2PO_4, 300 mM NaCl, 250 mM imidazole, pH = 8.0). To purify the protein from the pellet, a binding buffer (100 mM NaH_2PO_4, 10 mM Tris–Cl, pH = 8.0) with 8 M urea was added to the pellet. After stirring at room temperature for 30 min, it is centrifuged at 12 500 rpm for 30 min. The supernatant was transferred to another tube with Ni-NTA resin and shaking at room temperature for 1 h. After washing with a buffer (100 mM NaH_2PO_4, 10 mM Tris–Cl, pH = 6.3, 8 M urea), the protein was eluted with the elution buffer (100 mM NaH_2PO_4, 10 mM Tris–Cl, pH = 4.5, 8 M urea). The pH of eluates was adjusted to 8.0 by adding appropriate amount of Tris–Cl (pH = 8.8). The purified protein was checked by PAGE analysis and western blot (figures 2 and 3).

2.1.3. Extraction of crustacyanin. α-CRY and β-CRY pigments were extracted and purified from *Homarus Americanus* as follows: carapace shell was harvested from fresh lobster, washed very well, dried, ground and extracted

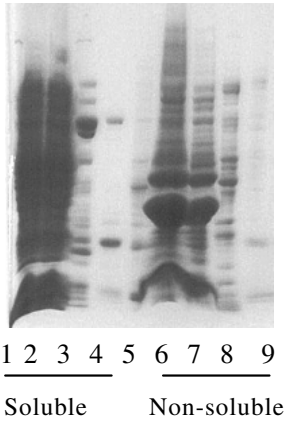

Figure 2. PAGE analysis after purification; 1–5, from soluble supernatant; 6–9, from pellet fraction; 1, lysate; 2, FT; 3, wash; 4 and 5, elute; 6, pellet; 7, FT; 8, pH = 6.3 elution; 9, pH = 4.5 elution. FT: flow-through.

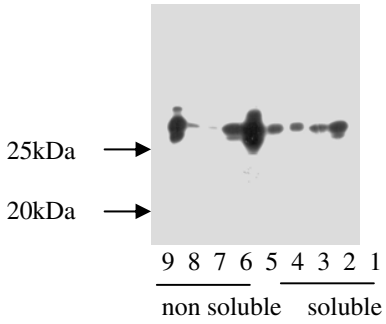

Figure 3. Western blot analysis using anti-His antibody after purification; 1–4, from soluble; 5–9, from non-soluble; 1, lysate; 2, FT; 3, wash; 4 and 5, elutes; 6, pellet; 7, FT; 8, elute at pH = 6.3; 9, elute at pH = 4.5.

with a borate buffer to remove impurities. The pigments were extracted with ethylenediaminetetraacetic acid (EDTA), precipitated with ammonium sulfate and purified by an anion exchange resin using a phosphate buffer. Several chromatography columns were run to develop the separation methodology. Peak fractions containing α-CRY and β-CRY were pooled, precipitated and re-suspended in the 0.1 M phosphate buffer. Excess of salt was not removed by dialysis, but rather by using slide-a-lyzer dialysis cartridges. Protein concentrations were estimated using the Bradford method with a BSA standard. CRY was also synthesized for comparison purposes.

2.1.4. Film processing. We have employed two processing techniques for the fabrication of ultrathin films of the proteins. In the SA technique, a monolayer of protein (AXT**,** HST and α- and β-CRY) was adsorbed onto an oxidized silicon substrate, ITO and gold interdigitated electrodes (IDEs) by the following procedure: the Si substrate was washed with a diluted acidic solution and then treated with a 7:3 concentrated sulfuric acid/hydrogen peroxide solution for 1 h. Further, the substrates are treated in 1:1:5 ammonium hydroxide/hydrogen peroxide/water for another hour. These substrates were cleaned using deionized water and dried by nitrogen flux. This procedure creates hydrophilic substrates. Later, the substrates were immersed in toluene for 2 h, and further treatment was performed to make the samples positively charged by immersing it in a solution of toluene with 5% of 3-[2-(2-aminoethyl)-ethylamino]-propyltrimethoxysilane (AEEA) for 24 h. After being rinsed sequentially with toluene, acetone and water and dried under a N_2 stream, the substrates were treated with γ-maleimidobutyric acid *N*-hydroxysuccinimide ester (GMBS), as a cross-linker between the sulfhydryls on the substrate and amino groups on the protein. After 1 h in 5 mM GMBS solution (dissolved in *N*,*N*-dimethylformamide and diluted with absolute ethanol), the substrates were washed with the phosphate buffer and then soaked in a 0.8 mg ml^{-1} solution of protein in the phosphate buffer.

In the LB deposition technique, films of α- and β-CRY were formed onto substrates by using the LB trough Type 612D, Nima Tech., UK. 1 M NaCl was used as subphase. Solutions of α- and β-CRY (0.8 and 0.6 mg ml^{-1}, respectively) were prepared in a pH = 7 phosphate buffer solution. Monolayers were compressed to the surface pressure of 16 mN m^{-1} which were previously determined from isotherm curves. The formation of layers (1 0 0) was performed by compressing the barriers to reach the surface pressure of deposition. The films were then transferred onto ITO, Si or IDE electrodes.

3. Results and discussion

The different materials were characterized using optical spectroscopy, fluorescence, FTIR and electrical measurements.

3.1. Optical spectroscopy

3.1.1. UV–visible spectra of AXT. Optical absorption characteristics spectra were evaluated at room temperature in different solvents such as chloroform, dimethylformamide, methylene chloride and ethanol. As film formation techniques vary according to solvent properties, solvents which have a high polarity index such as chloroform, have been used in our work. Absorption maxima range from 464 to 480 nm. A single broad absorption band is observed in almost every solvent used in this study except ethanol. AXT in ethanol shows an additional peak at 372 nm. The highest calculated coefficient value has been obtained for AXT in methylene chloride (1.778×10^5) and the lowest is found in ethanol (0.905×10^5). Figure 4 shows the optical spectra of AXT LB films on ITO and quartz, with characteristics that differ from those obtained in solution.

A HST film was cast from a 6×10^{-6} M solution on quartz and dried in vacuum for 1 h in the dark before the optical spectra were recorded (figure 5). Only one peak at 400 nm is observed.

Astaxanthin–histidine reaction: the carotenoid, held rigidly in its center by protein interactions, is hydrogen bonded via histidine and water respectively at the 4- and 4′-keto groups [7]. Commercial histidine is used to understand the spectral properties of β-CRY. Figure 6 suggests that the carotenoid is distorted by end ring flattening to extend the conjugation and

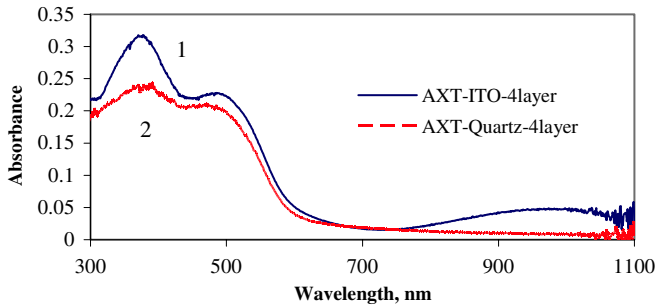

Figure 4. UV–visible spectra of LB films of AXT on ITO (1) and quartz (2).

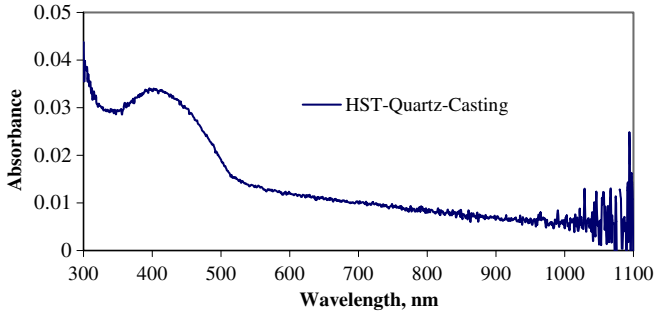

Figure 5. UV–visible spectra of a cast HST film on quartz.

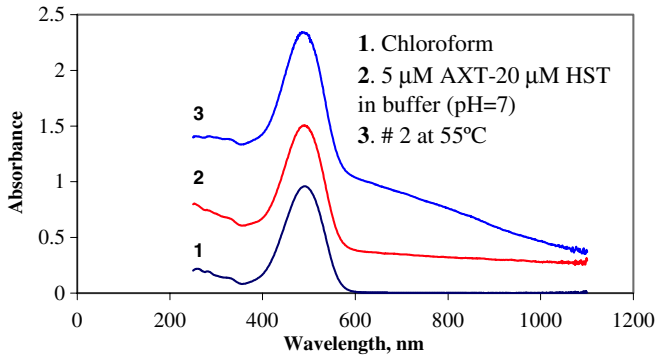

Figure 6. UV–visible spectra of AXT.

by bending. Thus, it is the way in which the protein subunits clamp the carotenoid molecules that determines their characteristic absorption and color.

Figure 7 shows the optical spectra of synthetic β-CRY in buffer solution where absorption increases with temperature (i.e. the 960 nm absorption band) and it is reversible. The lobster shell-derived β-CRY is an irreversible dissociation product of α-CRY and combinations of two types of $\approx$20 kDa promoters (apoproteins) with carotenoids [8–11]. Both pigments were characterized in a buffer solution (pH = 7) at room temperature and upon heating/cooling cycles. Figure 8 shows the optical spectra of both protein derivatives. α-CRY shows an absorption maximum at 607 nm, which can be irreversibly converted into a subunit, β-CRY ($\lambda_{max} = 579$ nm). These results are very similar to the results of Zagalsky and co-workers [12, 13]. While α-CRY is showing

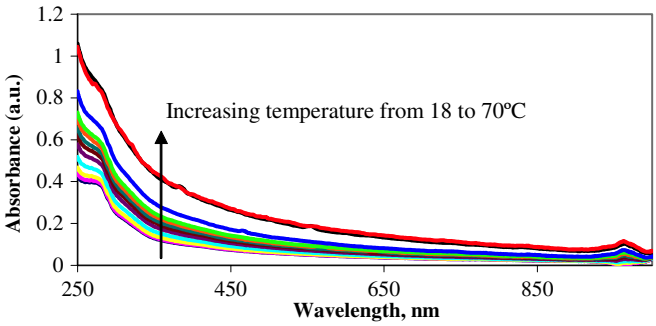

Figure 7. Optical spectra of synthetic β-CRY (0.3 mg ml^{-1}) upon temperature increase.

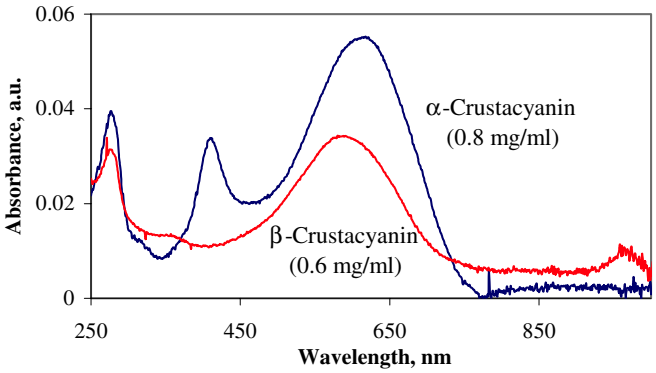

Figure 8. Optical spectra of α-CRY (0.8 mg ml^{-1}) and β-CRY (0.6 mg ml^{-1}) at RT.

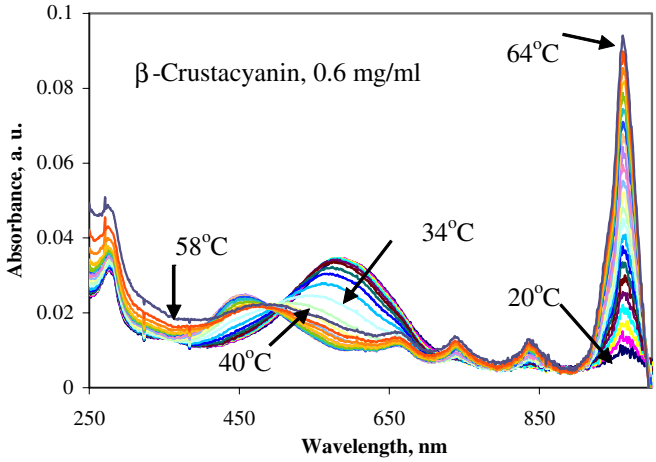

Figure 9. Optical spectra of β-CRY upon heating from 20 to 64 °C.

other peaks at 403 and 274 nm, β-CRY exhibits peaks at 274 nm, 456 nm (small and broad) and at 960 nm.

Lobster pigments are denatured to red products with spectra similar to AXT in the presence of non-polar denaturing agents or with temperature. Therefore, denaturation of α- and β-CRY as a function of temperature was studied here. Experiments are performed *in situ* to monitor the formation of the new molecule. Figure 9 shows the optical spectra of β-CRY with temperature. There is a gradual blue shift of the absorption maximum (574 nm) with a broadening of the 445 nm peak at 55 °C and a small increase and shift at 456 nm

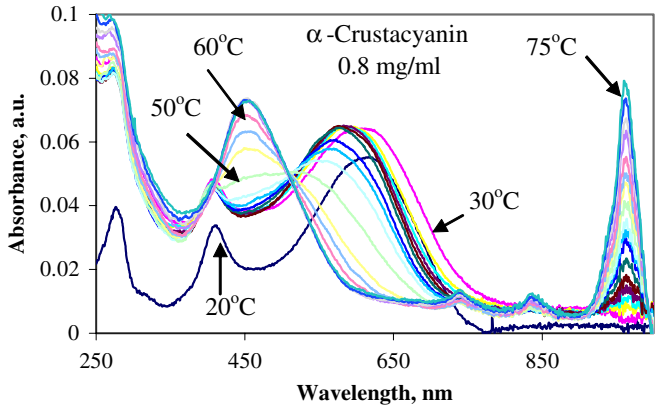

Figure 10. Optical spectra of α-CRY upon heating (20–75 °C).

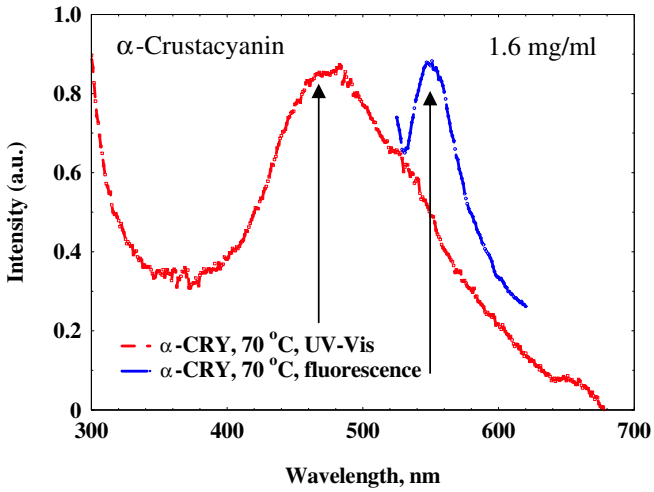

Figure 11. Fluorescence (excitation at 515 nm) and optical spectra of α-CRY after heating to 70 °C.

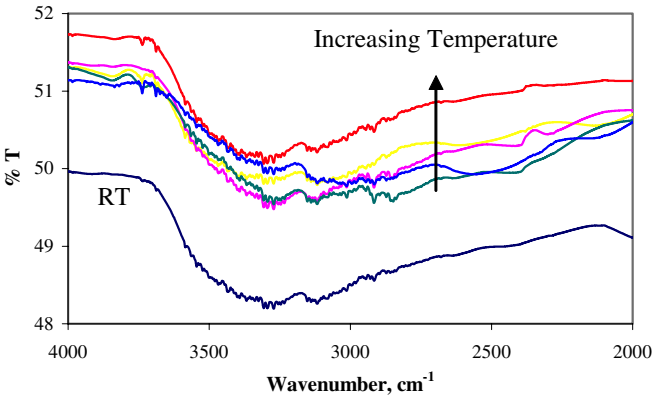

Figure 12. FTIR spectra of HST on ZnSe at RT, 35, 45, 55, 85 and 95 °C.

at 64 °C. Other absorption bands are observed with increasing temperature especially at 960 nm. In addition, smaller peaks are observed at 730 and 829 nm.

Denaturation of proteins can occur under a variety of physical conditions, including high temperature, very low or high pH and very high pressure. In many cases, the denaturation is only partially reversible; thermal denaturation in particular often results in irreversible inactivation. However, this can be remediated by limiting the operating temperature range and manipulating protein concentration. Also, to avoid irreversibility, the use of steam to sterilize enzyme reactors or enzyme sensor tips, which greatly limits their applications, is not recommended. Reaction reversibility is tested in the solution phase by optical spectroscopy and in the solid phase by FTIR spectroscopy.

The same solution is cooled down to room temperature (RT) and re-heated to check reversibility. The absorption bands at 730, 829 and 960 nm showed reversible absorption efficiency with temperature. This process was repeated three times and the same results were obtained. The new band position at 487 nm correlates with the absorption spectrum obtained for the AXT molecule in ethyl alcohol at around 470 nm and remained unchanged after heating and cooling repeatedly.

Figure 10 shows the effect of temperature on α-CRY. As we mentioned before, α-CRY shows different absorption characteristics than β-CRY and its response to temperature is also different. There is a gradual shift and increase in absorption band intensity at 607 nm. This band shifts to 456 nm at 50 °C and overlaps with the 403 nm band resulting in a broader one. Further increase in temperature results in line narrowing of the high intensity 445 nm band. The same bands observed in the β-CRY spectra are observed here as well at 730, 829 and 960 nm. Upon cooling and heating, the 445 nm band of α-CRY remains unchanged, but the peaks at 730, 829 and 960 nm showed a reversible behavior. According to the literature [14–17], these shifts are related to denaturation and re-positioning of the hydrogen atom closer to the C4 keto oxygen, or coplanar conformation of β rings adopted in the protein could contribute to the bathochromic shift. Given that most bluish pigments tend to have >11 conjugated double bonds, it is however possible that the calculations underestimate the effect of the end β rings being essentially coplanar with the polyene chain in the protein.

3.1.2. Fluorescence spectra of CRYs. The linear absorption spectrum is obtained for each sample before the emission spectrum is taken. β-CRY did not exhibit any fluorescence emission properties when excited at its maximum absorption peak at room temperature or when heated up to 70 °C. This is due to denaturation of β-CRY and release of AXT from the protein structure. Similarly, no emission was observed for α-CRY. However, emission with a maximum at around 560 nm was observed when the solution was heated to 70 °C (figure 11) and that the intensity is dependent on the excitation wavelength. At the molecular level, dehydration of the protein can lead to relaxation of the AXT molecule resulting in fluorescence.

3.1.3. FTIR spectroscopy. HST is widely used because quantum chemical studies showed that some of the structural perturbations contribute to the bathochromic shift of the absorption by AXT in β-CRY. Calculations suggest that this shift is largely due to one of the AXT C4 keto groups being

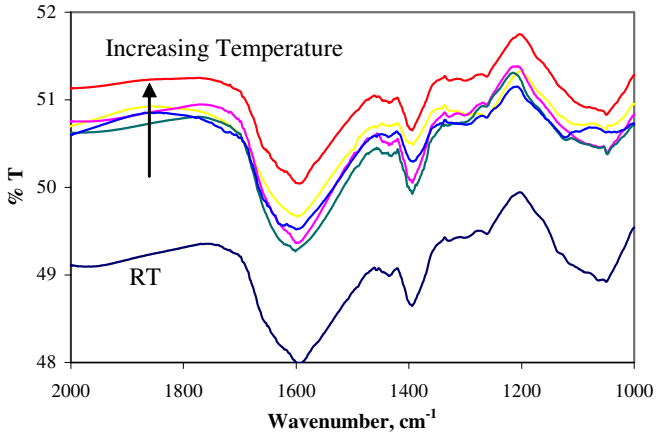

Figure 13. FTIR spectra of HST on ZnSe at RT, 35, 45, 55, 85 and 95 °C.

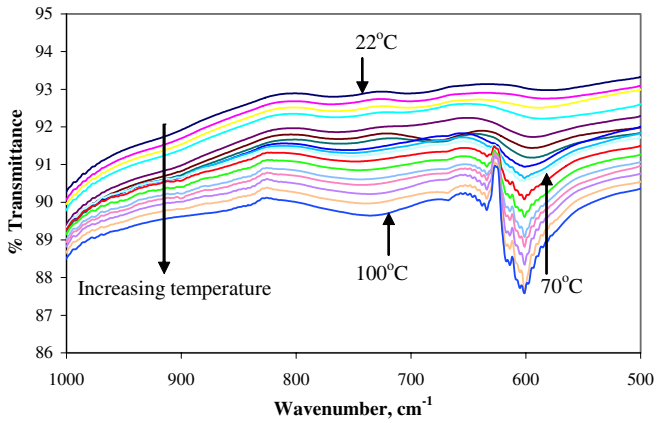

Figure 14. FTIR spectra of α-CRY on Si as a function of temperature.

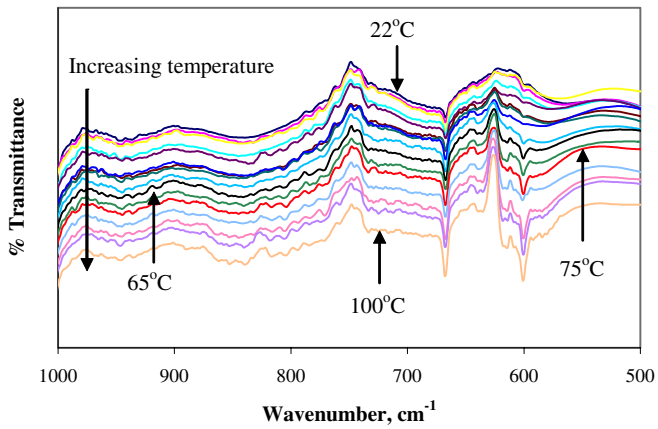

Figure 15. FTIR spectra of β-CRY on Si as a function of temperature.

hydrogen bonded to a HST residue of the surrounding protein, which results in the structural change of CRY [18].

Most of the IR bands of proteins are relatively broad. The best studied IR band of proteins is the amide I band appearing between 1600 and 1700 cm^{-1} with a maximum for most proteins at around 1654–1674 cm^{-1}, which arises

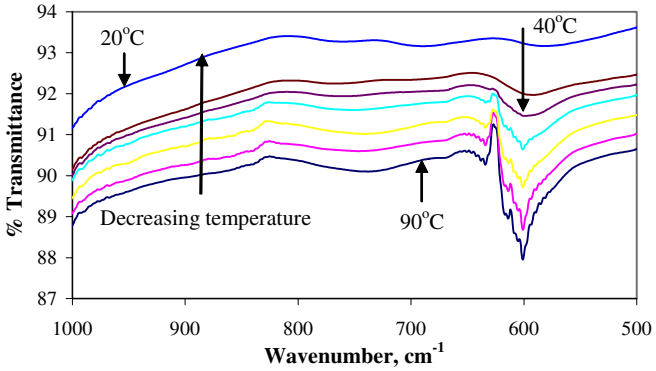

Figure 16. FTIR spectra of α-CRY on Si with decreasing temperature from 90 to 20 °C.

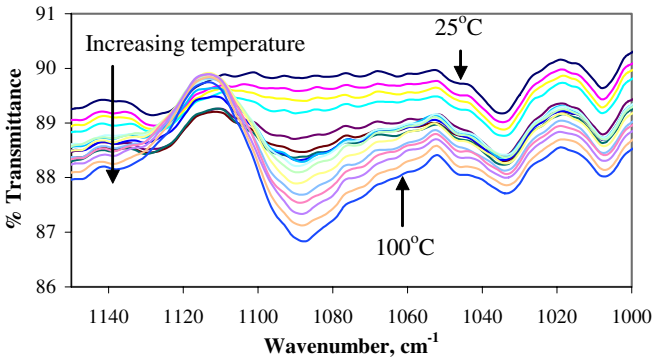

Figure 17. FTIR spectra of α-CRY on Si as a function of temperature (1000–1150 cm^{-1}).

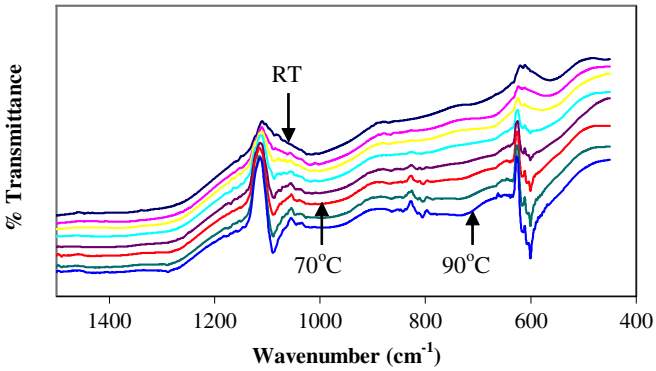

Figure 18. FTIR spectra of a 100-layer β-CRY on Si as a function of temperature (450–1500 cm^{-1}).

primarily from the stretch vibration of the peptide C=O group. The prepared films were kept under vacuum while examining their IR characteristics at different temperatures to check for any structural perturbation. We found that intensity of the IR bands decreased, and no new bands corresponding to disordered polypeptide appeared as the temperature was increased. FTIR spectra of HST were recorded for a sample prepared on ZnSe for two IR wave number ranges (1000–2000 and 2000–4000 cm^{-1}) for better resolution (figures 12 and 13). With increasing temperature, the peak intensity (% transmittance value) increases, but again no structural

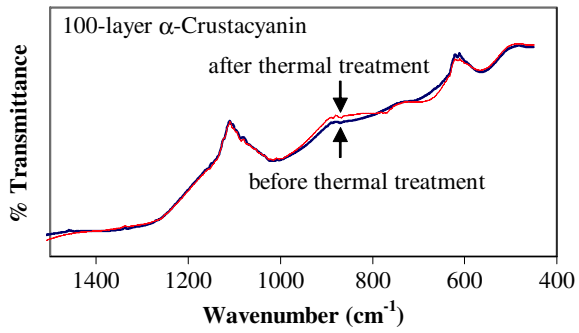

Figure 19. RT FTIR spectra of α-CRY on Si before and after thermal treatment.

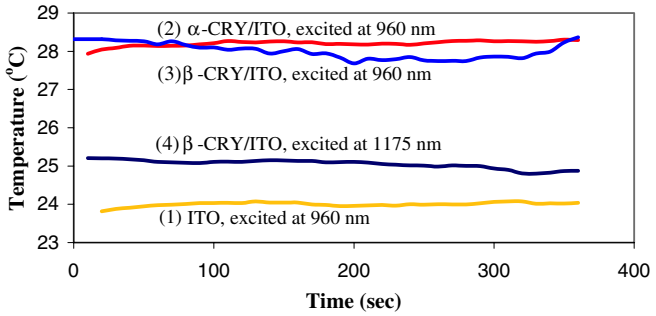

Figure 20. Femtosecond laser excitation of ITO (1) and CRYs coated on ITO.

differences are obtained due to heating. The peaks broaden however when the temperature reaches 95 °C.

Hydrogen bonding and dehydrogenation of CRYs derived from the lobster shell have been monitored as well. We did not observe any vibrational change in the 1600–1700 cm^{-1} range; however, the new peak at 601 cm^{-1} (16.6 μm) for both CRY forms on Si substrates evolves with temperature (figures 14 and 15). According to the literature [16] these peaks can be assigned to out-of-plane N–H bending and –OCN bending. These peaks are reversible; when the temperature decreases to room temperature, the peaks revert back to their initial positions (figure 16).

FTIR spectra of CRYs were recorded and studied in a narrower spectral range to follow the evolution/change of certain peaks. Figures 17 and 18 show spectra of α- and β-CRY at 1000–1150 cm^{-1} and 400–1450 cm^{-1}, respectively. Peak intensity increases with temperature and is wavenumber dependent. The 3800 cm^{-1} peak disappeared as the sample was heated; this peak is however reversible.

Hydrogen bonding and dehydrogenation of α-CRY prepared by LB on Si was monitored as well. The 1600–1700 cm^{-1} bands are not observed. Furthermore, we have observed the evolution of a band at 601 cm^{-1} (16.6 μm) upon heating of samples prepared by LB and SA techniques. As mentioned earlier, these peaks can be assigned to out-of-plane N–H bending and –OCN bending. These peaks are reversible; therefore, when the temperature decreases back to room temperature, the peaks revert back to their initial positions (figure 19).

3.1.4. Ti:sapphire laser measurements. A Ti:sapphire laser with the 80–120 fs pulse output in the near IR region (960 nm, with a power of 280 mW) was used to monitor the temperature variation. The samples were excited at 960 nm, and temperature differentiations were recorded. The reason for the excitation at 960 nm is to understand absorption peak properties at 960 nm recorded before by thermal excitation. This absorption showed reversible properties after thermal exposure. Figure 20 shows the results of our measurements. Excitation is applied to the uncoated ITO sample, and temperature remained around 24–25 °C. α- and β-CRY-coated samples were excited at 960 nm; ∼3 °C temperature increase was observed. An 1175 nm excitation was also used. The temperature remained around 25 °C (plot 4).

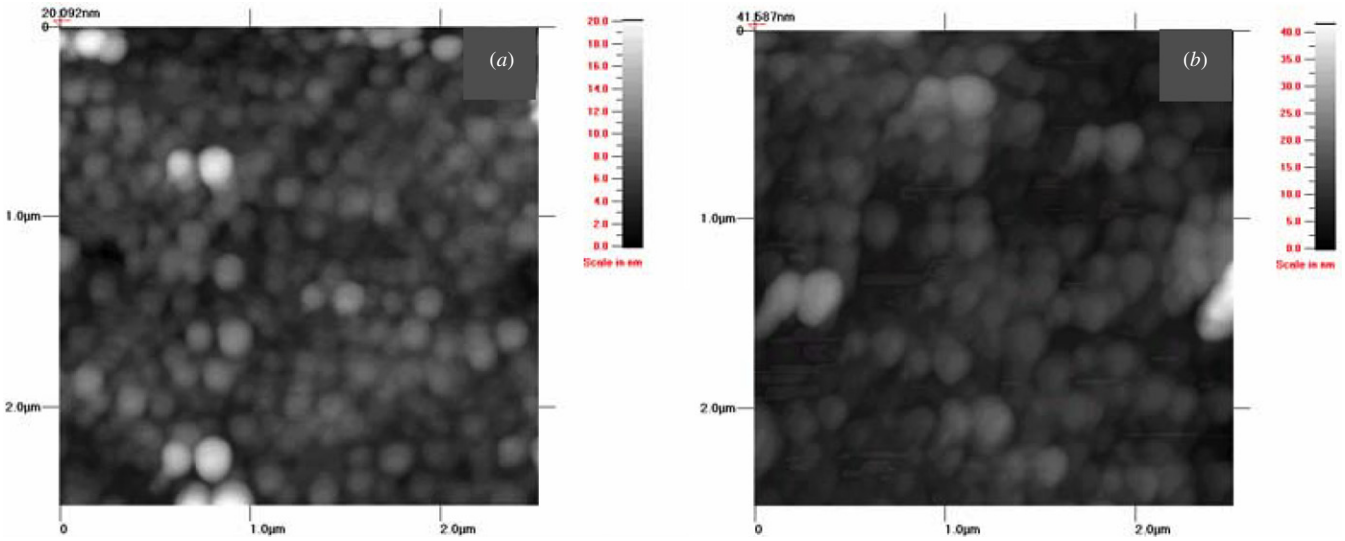

Figure 21. RT AFM of α-CRY on Si before (*a*) and after exposure to heat (b).

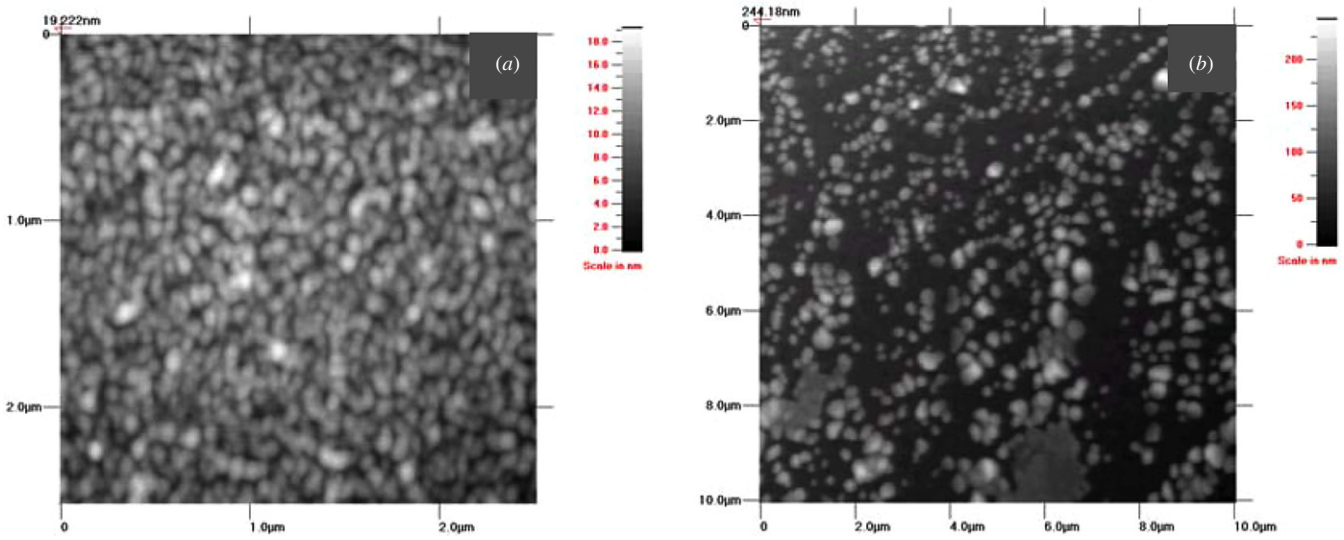

Figure 22. AFM of an SA film of α-CRY on an IDE (*a*) and LB film of β-CRY on an ITO electrode (b).

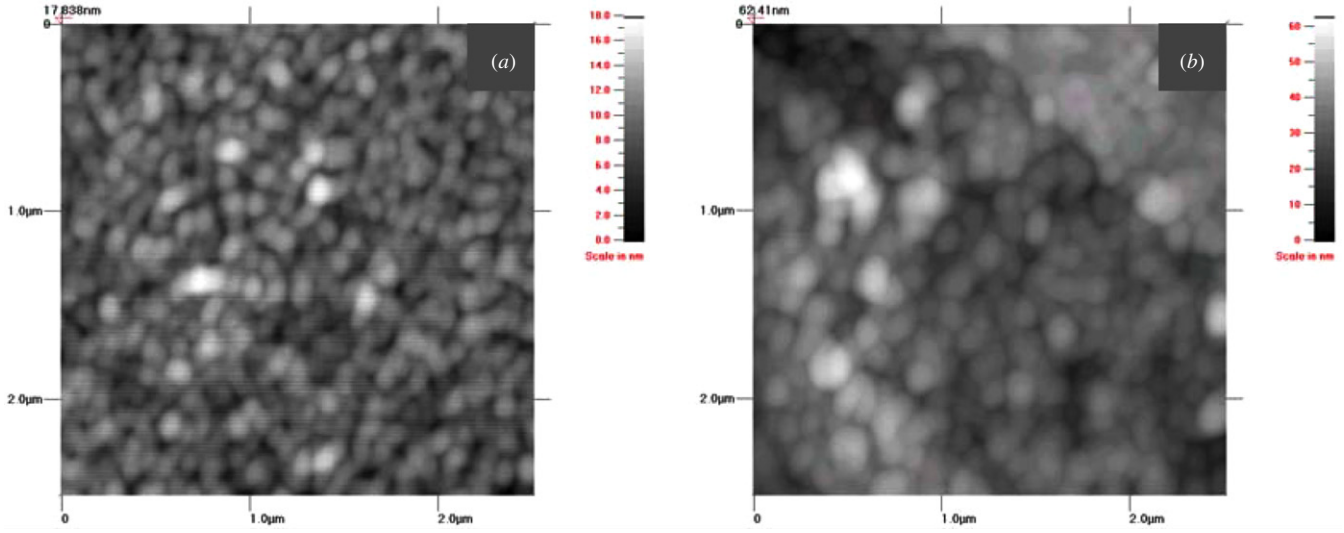

Figure 23. AFM of the α-CRY film after an applied potential (*a*) and after the laser exposure (*b*).

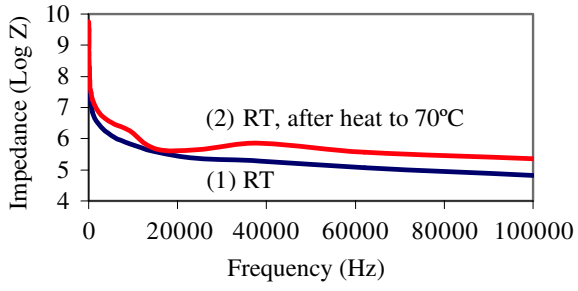

Figure 24. Impedance of α-CRY coated onto IDEs at RT before and after exposure at 70 °C.

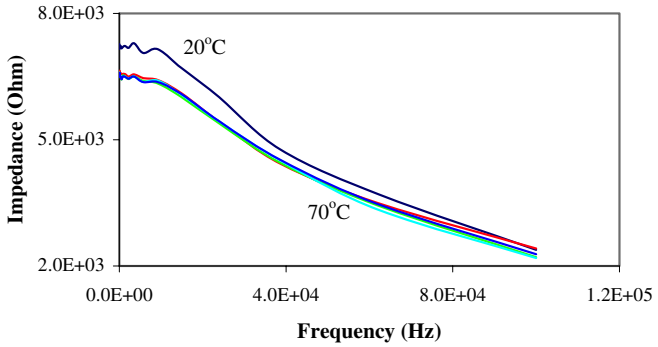

Figure 25. Impedance of α-CRY coated on ITO at different temperatures (20–70 °C).

3.1.5. Atomic force microscopy. Morphology and roughness are analyzed by atomic force microscopy (AFM) immediately after the films were prepared. Figure 21 shows a slight change in size and shape of the α-CRY pigment on Si substrates by heat.

Figures 22 and 23 show a slight change of the α-CRY particles of an SA film on Si substrates as a result of an applied potential and laser exposure. Similar characteristics for

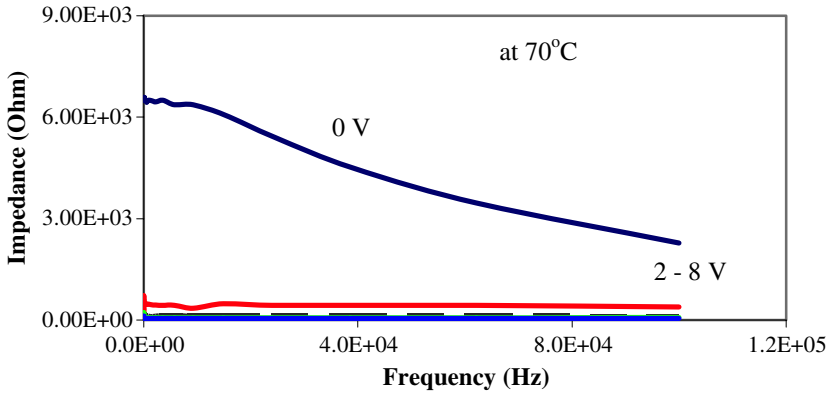

Figure 26. Impedance of α-CRY at 70 °C with an applied potential (0–8 V).

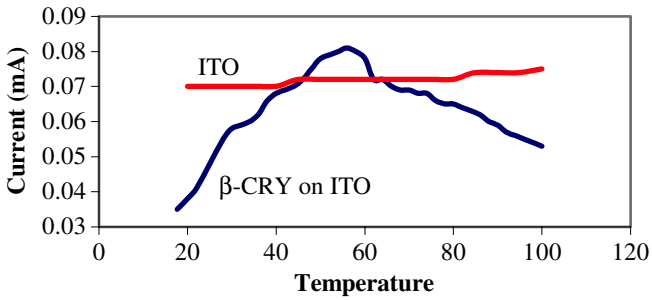

Figure 27. Current versus temperature of β-CRY on ITO.

β-CRY LB films were obtained. The slight difference between the AFMs of α-CRY and β-CRY is due to the difference in the preparation technique. As the high amount of salt is used for the subphase in LB, NaCl adsorbs into the protein layer, and this applies a surface pressure against the surrounding protein effectively squeezing the latter from the surface. The examination of a 15-layer SA protein film on a glass substrate showed that the average thickness per layer is around 1 nm.

3.1.6. I–V characteristics and impedance measurements. α- and β-CRY proteins were processed by SA and LB techniques onto ITO or IDEs for *I–V* characteristic and impedance measurements.

Impedance versus frequency was measured for an SA film of α-CRY at RT before and after heating to 70 °C. The experiment was run with no applied potential and at 1 V. The results shown in figure 24 indicate that there is a slight increase in impedance at 0 V as well as 1 V after the thermal treatment. However, measurements were repeated by variation of the applied voltage and *in situ* thermal heating. A 15-layer α-CRY on ITO was prepared by the SA technique. Heat was applied to the electrodes and impedance was measured when the temperature reached 70 °C, at different applied potentials (figures 25 and 26). Both measurements are resulted with an increase in impedance.

As any protein that has a large dipole moment in its native confirmation, it is likely to undergo a substantial change in conductivity when the native confirmation is significantly disrupted by a rise in temperature. *I–V* measurements were performed versus temperature of β-CRY deposited on ITO substrates (figure 27). The measurements were performed

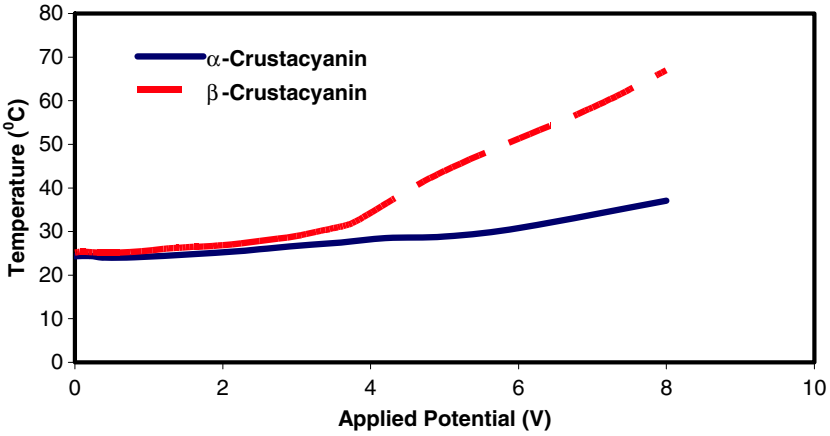

Figure 28. Temperature versus potential of SA films of crustacyanins on ITO.

on the protein coating sandwiched between the ITO and an aluminum foil, and current was measured as the temperature was varied. For baseline, the ITO electrode was heated up to 100 °C with no significant increase in its conductivity. However, upon a gradual increase of temperature to 60 °C of the β-CRY-coated ITO, the current increases from approximately 0.03 mA to 0.08 mA and then decreases slowly to 0.05, which is probably due to the conformational change. In the case of LB films of α-CRY coated onto IDEs, the temperature variation due to an applied current (0.01–0.05 μA) or voltage (0–14 V) was negligible (1 °C).

To reduce the electrode resistance, we have measured the cross-sectional resistance (z direction) by sandwiching the protein film between the ITO electrode on which it was deposited and an aluminum foil. Applied potential versus temperature data was plotted. As is seen in figure 28, a significant temperature increase for the α-CRY is observed (38 °C at 8 V), and a more significant increase is observed (65 °C at 8 V) in the case of β-CRY.

4. Conclusions

The numerous experiments we have carried out have shown that the crustacyanin protein is quite responsive not only in different ranges of the IR spectrum, an effect which is useful in IR detection and imaging applications, but also in the visible–near IR region. In addition, electrical response of the electrodes exhibited very promising results. *I–V* characteristics versus temperature showed that the protein can be used as an electro-optic thermal sensing device as well. The high sensitivity and fast response of the protein layer was further enhanced by the deposition process we used. The thin coatings prepared by LB or SA techniques exhibited the needed thermo-active response; however, SA films showed better thermal stability than the LB ones. Furthermore, the protein exhibited temperature variation under Ti:sapphire laser excitation at different wavelengths in ambient environment. We have also found that of the two forms, only α-CRY exhibited fluorescence properties after exposure to IR heat. Another characteristic that is of interest in this type of application is the stability of the protein structure after repeated heating/cooling cycles. We have conducted such experiments using the different characterization techniques mentioned above and we can conclude that this protein represents a formidable candidate for the fabrication of IR sensors.

The technology studied in this program will help to reevaluate uncooled IR detection and imaging technology by providing low cost, reliability and operational convenience with minimal sacrifice in performance for civilian and military applications. Another benefit of such biologically derived or inspired molecules will provide information for synthesis of proteins and amino acids. The recent advances toward the development of self-assembling polypeptide closed rings will make it possible to produce an entirely new class of artificial proteins. These nanoscopic proteins are referred to as protein nanotubes (PNTs) because they have open-ended hollow tubular structures. The interest in PNTs, which might be synthesized in the molecular structure, will open up the possibility for use in better performing IR detection and imaging devices in the future.

This technology will also be useful for waste management technology: (i) extraction of pigment containing crustacyanin from the sea animals, (ii) reuse of processed water and (iii) scale adsorption process technology would minimize the scale waste.

Acknowledgment

This work was sponsored by the US Air Force (AFRL/MLPJ), contract no. FA8650-04-M-5406.

References

[1] Tanaka A *et al* 1996 *IEEE Trans. Electron Devices* **43** 1844–50
[2] Liddiard K C 1986 *Infrared Phys.* **26** 43–9
[3] Oliver A D and Wise K D 1999 *Sensors Actuators* A **73** 222–31
[4] Choi I H and Wise K D 1986 *IEEE Trans. Electron Devices* **33** 72–9
[5] Beratan H, Hanson C and Meissner E G 1994 *Proc. SPIE* **2274** 147–56
[6] Tanaka A *et al* 1997 *Proc. SPIE* **3061** 198–209
[7] Wald G, Nathanson N, Jencks W P and Tarr E 1948 *Biol. Bull.* **95** 249
[8] Britton G, Armitt G M, Lau S Y M, Patel A K and Shone C C 1982 *Carotenoid Chemistry and Biochemistry* ed G Britton and T W Goodwin (Oxford: Pergamon) pp 237–53
[9] Zagalsky P F 1995 *Carotenoids* vol 1A ed G Britton, S Liaaen-Jensen and H Pfander (Basel: Birkhäuser) pp 287–94
[10] Zagalsky P F, Eliopoulos E E and Findlay J B C 1990 *Comp. Biochem. Physiol.* B **97** 1–18
[11] Quarmby R, Norden D A, Zagalsky P F, Ceccaldi H J and Daumas R 1977 *Comp. Biochem. Physiol.* **56B** 55–61
[12] Zagalsky P F 1976 *Pure Appl.Chem.* **47** 103
[13] Zagalsky P F, Eliopoulos E E and Findlay J B C 1990 *Comp. Biochem. Physiol.* **97B** 1
[14] Buchwald M and Jencks W P 1968 *Biochemistry* **7** 844
[15] Buchwald M and Jencks W P 1968 *Biochemistry* **7** 834
[16] Cianci M, Rizkallah P J, Olczak A, Raftery J, Chayen N E, Zagalsky P F and Helliwell J R 2002 *Proc. Natl Acad. Sci. USA* **99** 9795
[17] Weesie R J, Merlin J C, Lugtenburg J, Britton G, Jansen F J H M and Cornard J P 1999 *Biospectroscopy* **5** 19
[18] Durbeej B and Eriksson L A 2003 *Chem. Phys. Lett.* **375** 30